A priori method for propensity rules for inelastic electron tunneling spectroscopy of single-molecule conduction

Alessio Gagliardi,[1,2] Gemma C. Solomon,[3,6] Alessandro Pecchia,[4] Thomas Frauenheim,[1] Aldo Di Carlo,[4] Noel S. Hush,[5,6] and Jeffrey R. Reimers[6]

[1]*Bremen Center for Computational Materials Science, University of Bremen, D-28359, Germany*

[2]*PaSCO Graduate School, University of Paderborn, D-33098 Paderborn, Germany*

[3]*Department of Chemistry, Northwestern University, 2145 Sheridan Road, Evanston, Illinois 60208-3113, USA*

[4]*CNR-INFM Dep. of Electronics Engineering, University of Rome "Tor Vergata," Via del Politecnico 1, 00133, Italy*

[5]*School of Molecular and Microbial Biosciences, The University of Sydney, Sydney, New South Wales 2006, Australia*

[6]*School of Chemistry, The University of Sydney, Sydney, New South Wales 2006, Australia*

(Received 8 January 2007; revised manuscript received 18 February 2007; published 25 May 2007)

An *a priori* computational method for determining intensities in inelastic electron tunneling spectroscopy (IETS) is developed that allows simple, chemically intuitive propensity rules to be obtained for arbitrary applications. The molecule is shown to scatter charges between quite specific eigenchannels of lead-coupling-weighted molecular density of states. This allows mode-specific scattering sites to be identified within the molecule, indicating how external chemical or other perturbations could be used to control IETS intensities.

I. INTRODUCTION

Since the original paper of Aviram and Ratner[1] which showed the theoretical possibility of molecular electronic devices, many advances have been made. Despite this progress the challenge in making robust scientific or commercial devices remains considerable. In the last few years much effort has been devoted to investigating dissipation processes in molecular electronic devices[2–4] and inelastically scattered electrons can be used directly as probes to investigate many properties of the device itself using the inelastic electron tunneling spectroscopy (IETS) technique.[5,6] While this technique is quite old,[7] it has not been popular until now for two main reasons. First, compared with other more traditional spectroscopic techniques like infrared spectroscopy, high-resolution electron energy loss spectroscopy (HREELS), or Raman spectroscopy, IETS has a more complicated setup for measurements as the sample must be connected between two electrodes. Second, the spectra have been difficult to interpret because IETS does not have definite selection rules[8–12] and also because it is difficult to isolate the influence of the environment and local structural variations on the final spectra. While the advent of experimental molecular electronics has solved the first issue, the influence of the environment is still an open question. Many groups have investigated the rigorous formalism which underlies IETS measurements,[2,9,13–17] while Troisi and Ratner[12,18] and Lorente *et al.*[9] have developed some intuitive propensity rules that capture many of the features that lead to vibrational-mode selectivity in IETS. The main aim of the present work is to present a general approach to the interpretation of IETS measurements, starting with fundamental principles implemented using a generally applicable *a priori* computational scheme. Further, a simplified form of the inelastic current will be derived and justified. Finally, it will be shown how not only the propensity rules of Troisi and Ratner may be rigorously derived but also enhancing these rules. This can provide a thorough, yet easily, understood descrip-

tion of the general phenomenon that may be readily applied in diverse practical applications.

II. THEORETICAL METHOD

Our calculations are performed using the Green's function density-functional tight-binding (GDFTB) program[17,19] that implements the nonequilibrium Green's function (NEGF) technique for calculating the elastic and inelastic currents that flow in a molecular-electronic device. The zeroth-order Hamiltonian for the system, including the two contacts, is computed *a priori* using the standard DFTB method[20] implemented in a local-orbital basis. All effects including steady-state heating of the device and the possibility of phonon emission at high temperature are included in this fully general formalism. The flow of current is obtained from the Meir-Wingreen equation[21]

$$I = \frac{2e}{h} \int_{-\infty}^{+\infty} \text{Tr}[\Sigma_L^<(E)G^>(E) - \Sigma_L^>(E)G^<(E)]dE, \quad (1)$$

where the $G^{<(>)}(E)$ lesser (greater) Green's functions describe the distribution of occupied (empty) states in the system and satisfy the kinetic equations:

$$G^{\langle,\rangle}(E) = G^r(E)[\Sigma_L^{\langle,\rangle}(E) + \Sigma_R^{\langle,\rangle}(E) + \Sigma_{el\text{-}ph}^{\langle,\rangle}(E)]G^a(E). \quad (2)$$

The first two terms which appear in Eq. (2) are the lesser (greater) self-energies which take in account the effect on the distribution of electrons induced by the open boundary conditions:

$$\Sigma_{L,R}^{\langle,\rangle}(E) = \eta^{\langle,\rangle}[-2\,\text{Im}\{\Sigma_{L,R}^r(E)\}] = \eta^{\langle,\rangle}\Gamma_{L,R}, \quad (3)$$

where $\eta^{<(>)}$ is equal to $if_{L,R}$ ($-i(1-f_{L,R})$) and f are the Fermi distribution functions for the contacts. The third term $\Sigma_{el\text{-}ph}^{<,>}$ introduces the inelastic scattering in the current and embodies the electron-phonon interaction. It is computed using a Dyson perturbation expansion truncated at first order (the

Born approximation) as the interaction between the electrons and phonons is assumed to be weak, producing

$$\Sigma_{el\text{-}ph}^{\langle,\rangle}(E) = \sum_q \frac{i}{2\pi} \int_{-\infty}^{\infty} \alpha_q G_0^{\langle,\rangle}(E-E') \alpha_q D_q^{\langle,\rangle}(E') dE, \quad (4)$$

where α_q is the electron-phonon coupling matrix defined by

$$\alpha_q = \frac{\partial H}{\partial Q_q} - \frac{\partial S}{\partial Q_q} S^{-1} H - H S^{-1} \frac{\partial S}{\partial Q_q} \quad (5)$$

for vibrational mode q with normal mode Q_q and molecular Hamiltonian H and orbital overlap S.[17] As IETS measurements are performed at very low temperature (usually 4 K), we can simplify Eq. (4) assuming temperature $T=0$. We also approximate the phonon population to a collection of Einstein oscillators in thermodynamic equilibrium with the environment. Under this approximation, at $T=0$, the population of phonons N_q, is set to zero and Eq. (4) becomes

$$\Sigma_{el\text{-}ph}^{\langle,\rangle}(E) = \alpha_q G_0^{\langle,\rangle}(E \pm \omega_q) \alpha_q \quad (6)$$

where the upper (lower) sign is for the lesser (greater) self-energy and $G_0^{<,>}$ are the zeroth-order lesser or greater Green's functions obtained in the absence of electron-phonon coupling. The current from Eq. (1) thus becomes, expanding up to the second order in α_q,

$$I = \frac{2e}{h} \int_{\mu_R}^{\mu_L} \left(\text{Tr}[\Gamma_L G_0^r \Gamma_R G_0^a] + \sum_q \text{Tr}[\Gamma_L G_0^r \Sigma_{ph}^r G_0^r \Gamma_R G_0^a] \right.$$

$$\left. + \text{Tr}[\Gamma_L G_0^r \Gamma_R G_0^a \Sigma_{ph}^a G_0^a] dE \right) + \sum_q \Theta(\mu_L - \mu_R$$

$$- \omega_q) \frac{2e}{h} \int_{\mu_R+\omega_q}^{\mu_L} \text{Tr}[\Gamma_L G_0^r \alpha_q \tilde{G}_0^r \tilde{\Gamma}_R \tilde{G}_0^a \alpha_q G_0^a] dE = I_{el}$$

$$+ \sum_q \Theta(\mu_L - \mu_R - \omega_q) I_q, \quad (7)$$

where

$$I_q = \frac{2e}{h} \int_{\mu_R+\omega_q}^{\mu_L} \text{Tr}[\Gamma_L G_0^r \alpha_q \tilde{G}_0^r \tilde{\Gamma}_R \tilde{G}_0^a \alpha_q G_0^a] dE. \quad (8)$$

The first three terms of Eq. (7) represent the coherent current, including part of the virtual electron-phonon scattering terms, whereas the latter term is the inelastic (incoherent) current component. Moreover, it is assumed that $\mu_L > \mu_R$, implying that electrons are flowing from the left to the right contact. In order for phonon emission to take place, the applied bias must obey the condition $\mu_L - \mu_R > \omega_q$, which is emphasized by the Heaviside function in front of the inelastic component. The use of the zeroth-order Green's functions in Eq. (7) is a valid approximation, because the electron-phonon interaction is small in the system considered here. Numerical calculations, including the renormalization of the propagators, lead to essentially the same incoherent current, to within few percent of errors.

The first three terms in Eq. (7) give a coherent contribution, describing the elastic part of the current, while the last term is the inelastic component expressed as the sum of independent contributions, I_q, from all of the vibrational modes
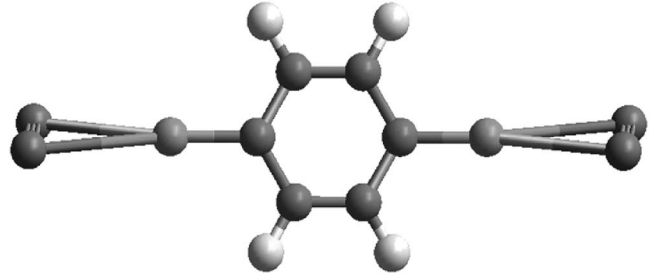

FIG. 1. A chemisorbed 1,4-benzenedithiol molecule connected to two gold atoms on each side.

of the molecule. In the inelastic term the matrices with a tilde are computed at an energy shifted by the energy of a phonon: $E' = E - \omega_q$. The shift comes from the conservation of energy and in fact describes the lowering of the energy of the electron after the excitation of a phonon. We hence see that the inelastic current depends on five basic quantities: the propagators $G_0^{r,a}$, the vibronic coupling matrix α_q, the vibrational frequency ω_q, the couplings between the contacts and the molecule, $\Gamma_{L,R}$, and the Fermi energy E_F. The main question is, of course, what are the relationships between these quantities and how we can simplify the picture in order to have a better insight into the physics involved?

III. DEFINITION OF TRANSMISSION CHANNELS

The specific system investigated in this study is the 1,4-benzenedithiol molecule chemisorbed between two gold contacts, though the applications of the method presented are quite general. As we have already demonstrated that the symmetry properties of coherent transport through gold-thiol junctions are dominated by the molecular symmetry[22] and that low-dimensional models of the electrode capture most of the essential features of observed IETS;[17] we use just two atoms to represent each lead, as shown in Fig. 1. This interface structure is the one predicted to be the lowest energy using density-functional theory calculations,[23] although experimental evidence implies top-site binding for alkylthiols.[24,25] The low-temperature IETS spectrum calculated using only the Born approximation is shown and assigned in Fig. 2. We seek a basic understanding of how this spectrum arises and the relative propensities calculated for the modes. The chemisorbed 1,4-benzenedithiol molecule has d_{2h} symmetry, and the IETS-active modes are categorized in Fig. 2 accordingly: the most prominent modes are in-plane totally symmetric a_g modes while the out-of-plane antisymmetric b_{2g} and b_{3u} modes are also significant. However, the conduction process depicted by Eq. (7) does not display d_{2h} symmetry as the $\Gamma_{L,R}$ matrices have only the symmetry of the left and right junctions, not the full molecular or device symmetry.[22] Analysis of Eq. (8) thus must commence with this reduced symmetry, the *conductance point-group* symmetry which, in this case, is C_{2v} (Ref. 22); note that lowercase symbols are used throughout for the description of molecular symmetry while uppercase symbols are used for the description of molecular-conductance symmetry. We must demonstrate how IETS appears to take on the mo-
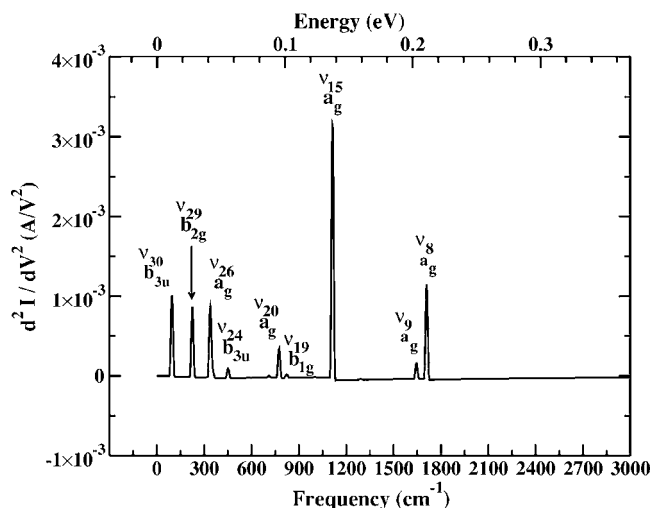
FIG. 2. The IET spectrum of our system. The broadening of the peaks has been introduced empirically considering a phonon lifetime of 6.6×10^{-13} s, corresponding to a broadening of 2×10^{-3} eV.

FIG. 3. (Color online) The energy dependence around the Fermi energy E_F for the eigenvalues $\hat{\Gamma}_{ii}^L$ of Γ_L (top) and $\bar{A}_{ii}^L$ of $\bar{A}^L$ (bottom) partitioned into symmetry components.

lecular symmetry properties in spite of this limitation.

Our approach is based on the idea that both the elastic and inelastic current can be expressed as the sum of a small number of essentially noninteracting paths or channels through the device. This has been recently demonstrated[26] by us for elastic transport through the introduction of the transformation

$$\hat{\Gamma}_{L,R} = B_{L,R}^{\dagger} \Gamma_{L,R} B_{L,R}, \qquad (9)$$

which reduces the electrode-molecule coupling matrices to diagonal form, a transformation that captures the essence of the physical insight used previously by Troisi and Ratner[12,18] in their proposed IETS propensity rules. After this transformation is applied we get the following formula for the inelastic current of every mode:

$$I_q = \frac{2e}{h} \int_{\mu_R + \omega_q}^{\mu_L} \left(\sum_{ij} \hat{\Gamma}_{ii}^L \hat{\Gamma}_{jj}^R (E - \omega_q) |\hat{\Lambda}_{ij}|^2 \right) dE, \qquad (10)$$

where $\hat{\Lambda} = \hat{G}_0^r \hat{\alpha}_q \hat{G}_0^r (E - \omega_q)$. As this diagonalization procedure does not take into account the orbital overlap, the eigenvalues $\hat{\Gamma}_{ii}^L$, etc., are not guaranteed to be positive definite, but in practice we find only a single negative eigenvalue whose magnitude is 12 orders of magnitude smaller that the dominate eigenvalue, thus allowing each individual contribution from $|\hat{\Lambda}_{ij}|^2$ to be interpreted as comprising a separate conductance channel. Note that neglect of the overlap during this procedure is essential to ensure that only the modulus of the $\hat{\Lambda}_{ij}$ terms appears in the equation.[26] This step does not constitute an approximation but rather provides an exact expression that tolerates a small amount of unexpected complexity in one part (the eigenvalues $\hat{\Gamma}_{ii}^L$) in order to obtain a dramatic simplification in another ($|\hat{\Lambda}_{ij}|^2$). Even with this additional compexity, the $\Gamma_{L,R}$ matrices are of very low rank because they contain information about the junction between
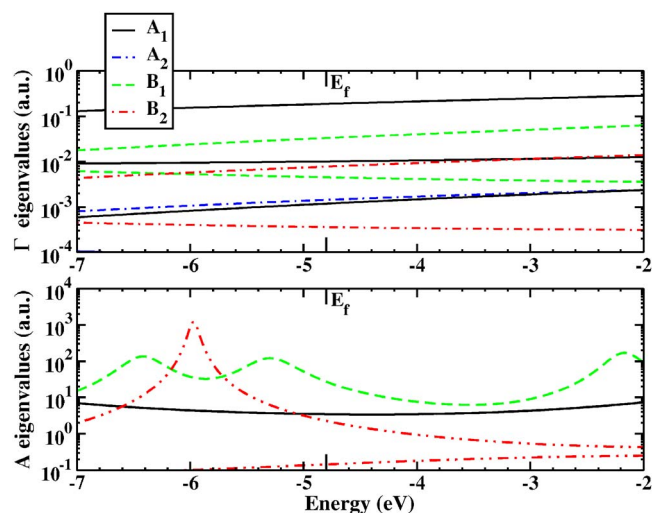
the sulfur group and the gold contact. This causes the spectrum of eigenvalues to possess only a few nonzero terms, indeed strictly only one nonzero term if just one sulfur orbital links the molecule to the lead.[26] While this result is obtained using a careful partitioning of the device into molecular and contacts region at the gold-sulfur junction, it remains valid even when a large number of gold atoms are included within an "extended molecule" in calculations designed to reach quantitative accuracy.[22]

The above junction channels will provide a good simple description of the (elastic or inelastic) conduction process whenever the bottleneck between the molecule and its contacts is the most important physical element. In this depiction, $|\hat{\Lambda}_{ij}|^2$ determines the probability that an electron or hole that enters the molecule from left lead through channel i is scattered inelastically out the right lead through channel j. In Fig. 3, upper section, we plot the amplitude $\hat{\Gamma}_{ii}^L$ for an electron entering the molecule in a window of energy of 5 eV encompassing the Fermi energy. The eigenvalues show a very low dependence on energy as the s-band density of states of the gold contacts is nearly energy independent. The graph shows also that effectively only one junction channel, of symmetry A_1 in the molecular-conductance point group, dominates the process, with the next most significant channel being of B_1 symmetry but an order of magnitude less transmissive. This result suggests that the most intense IETS process is likely to involve electrons or holes entering and exiting through the dominant A_1 left and right junction channels, respectively, a process that is only possible when vibrations of A_1 symmetry are involved. While this argument correctly predicts the propensity for a_g modes apparent in Fig. 2, the dominant process is actually found to involve the *less* transmissive B_1 channels of the left and right junctions. This shows that the $\hat{\Lambda}$ matrix, which contains information about the chemical properties of the molecule, also plays an important role in selecting which channel is the most important for the current, a role that arises as the conduction in the mol-

TABLE I. All significantly large eigenvalues of the electrode-coupling weighted density of states, $\bar{A}_{ii}^{L}$, at the Fermi energy E_F from Fig. 3.

Label	$A_{ii}^{L}(E_F)$
$1A_1$	3.44
$2A_1$	0.144
$3A_1$	0.0128
$1A_2$	0.0107
$1B_1$	27.4
$2B_1$	0.0705
$1B_2$	2.26

ecule near the Fermi energy of chemisorbed 1,4-benzenedithiol is dominated by the electronic π system that embodies B_1 but not A_1 symmetry.

The promise of this approach points to the possibility that a new set of "channels" might preserve all the nice characteristics of the previous ones, but allow for better insight into the role of the molecular properties. Our proposal lies in a second transformation based on diagonalization of the matrices $A^R = G_0^r \Gamma_R G_0^a$ and $(A^L)^* = G_0^a \Gamma_L G_0^r$:

$$\bar{A}^R = C_R^\dagger A^R C_R,$$

$$\bar{A}^L = C_L^\dagger (A^L)^* C_L. \qquad (11)$$

The conjugation of A^L arises because the Hamiltonian is a real matrix and therefore $(G_0^r)^\dagger = (G_0^r)^* = G_0^a$. Moreover, due to the fact that A^L is a Hermitian positive-definite matrix, the conjugation does not change its positive and real eigenvalues.

Although in this derivation we have used the unrenormalized propagators, the approach is quite general since Eq. (8) is valid also in the so-called self-consistent Born approximation (SCBA), provided all $G_0^{r,a}$ are substituted by renormalized propagators $G^{r,a}$. The electron-phonon self-energy $\Sigma_{el-ph}^{r,a}$ does not reduce further the symmetry of $(A_L)^*$ and A_R.

These matrices depict the coupling-weighted molecular density of states[27] and contain information about not only the junctions but also the chemical properties of the molecule as well. In Fig. 3, bottom section, we plot the eigenvalues $\bar{A}_{ii}^{L}$ where they may be compared to those previously discussed for $\hat{\Gamma}_{ii}^{L}$. The first thing we can observe is that a strong energy dependence appears with the $\bar{A}_{ii}^{L}$ eigenvalues showing peaks close to the energies of the molecular orbitals. The dominant eigenvalues at the Fermi energy are listed in Table I and, as expected, by far the largest eigenvalue is found to be of B_1 symmetry, named $1B_1$. Hence this new transformation provides improved insight into the physical problem of IETS scattering. The inelastic conductances are then given by

$$g_q = \sum_{ij} \bar{A}_{ii}^{L} \bar{A}_{jj}^{R} (E - \omega_q) \bar{\alpha}_{ij}^{q} \bar{\bar{\alpha}}_{ji}^{q}, \qquad (12)$$

where

$$\bar{\alpha}^q = C_L^\dagger \alpha_q C_R \quad \text{and} \quad \bar{\bar{\alpha}}^q = C_R^\dagger \alpha_q C_L. \qquad (13)$$

Differently from the Γ transformation the A matrices are positive definite and so their rotation should preserve this property. A subtlety, however, is that due to the differing energy dependences of Γ_L and Γ_R apparent in Eq. (8), the eigenvectors C_L and C_R are not simply related to each other so that $\bar{\alpha}_{ij}^{q}$ and $\bar{\bar{\alpha}}_{ji}^{q}$ become unrelated complex quantities and hence the ij contributions in Eq. (12) cannot strictly be interpreted as independent channels.

Nevertheless, in Table II the major contributions to g_q evaluated at the Fermi energy from the double sum of Eq. (12) are listed and at most two contributions account for at least 95% of the IETS signal. Single significant contributions are found only for the case of totally symmetric vibrations (a_g symmetry in the full molecular point group), these involving an electron entering through the $1B_1$ "channel" of the left lead, scattering off an a_g vibration and exiting through the $1B_1$ "channel" of the right lead. Otherwise, closely related pairs of contributions are involved, with, for example, the intense b_{2g} mode ν_{29} activated by a 50% contribution from an electron that enters the $1A_1$ "channel" and exits the $1B_1$ "channel" combined with a 45% contribution from an electron that enters the $1B_1$ "channel" and exits the $1A_1$ "channel."

The analysis presented in Table II presumes that the total IETS signal I_q from Eq. (7) can be approximated from the inelastic scattering conductance g_q evaluated only at the Fermi energy E_F. To test this hypothesis, the relative values of the total inelastic currents calculated using Eq. (7) and its approximation are given in the table where they are seen to be in very good agreement. The lack of symmetry in the leading terms shown in the table arises due to the shift ω_q that must be applied to the outgoing channel energies. Owing to the large values of the active frequencies compared to the energy dependences depicted in Fig. 4, such differences appear profound and indeed result in factors of two differences between the displayed eigenvalues $\bar{A}_{ii}^{L}(E_F)$ and the analogous values of $\bar{A}_{ii}^{R}(E_F - \omega_q)$. However, Troisi and Ratner[12,18] have argued that such changes should not qualitatively affect IETS propensity rules and hence we present in Table II an approximate analysis of g_q based on this further approximation. Indeed, the relative propensities evaluated using this crude approximation differ by at most 20% from the exact intensities I_q, indicating its usefullness. Further, this approximation leads to the reexpression of Eq. (12) in terms of true channels as

$$g_q = \sum_{ij} \bar{A}_{ii}^{L} \bar{A}_{jj}^{R} |\bar{\alpha}_{ij}^{q}|^2 \qquad (14)$$

and the dominant terms in these sums, now symmetrically disposed towards both leads, are also shown in Table (2). Further, this approximation facilitates the rewriting of Eq. (8) in the simple form

TABLE II. Properties of some significant IETS active vibrational modes q of frequency ω and symmetry as specified in the molecular point group (conductance point group), including the relative total intensity I_q from Eq. (7), the relative zero-voltage conductance g_q from Eq. (8) evaluated at the Fermi energy E_F, and the identity and contribution of its most significant channel contributor(s), and that as obtained approximately through the replacement of $\bar{A}^R(E-\omega_q)$ with $\bar{A}^R(E)$.

		Vibration q					$g_q(E_F)$ exact					$g_q(E_F)$ approximate			
ν	ω (eV)	ω (cm^{-1})	$d_{2h}(C_{2v})$	I_q Total	Total	Channel	%	Channel	%	Total	Channel	%	Channel	%
30	0.014	112	b_{3u} (B_1)	0.269	0.209	$1A_1 \rightarrow 1B_1$	48	$1B_1 \rightarrow 1A_1$	46	0.288	$1A_1 \rightarrow 1B_1$	48	$1B_1 \rightarrow 1A_1$	48
29	0.028	228	b_{2g} (B_1)	0.189	0.173	$1A_1 \rightarrow 1B_1$	50	$1B_1 \rightarrow 1A_1$	45	0.229	$1A_1 \rightarrow 1B_1$	48	$1B_1 \rightarrow 1A_1$	48
26	0.043	346	a_g (A_1)	0.199	0.175	$1B_1 \rightarrow 1B_1$	97.9			0.225	$1B_1 \rightarrow 1B_1$	98		
25	0.045	365	a_u (A_2)	0.032	0.027	$1B_1 \rightarrow 1B_2$	49	$1B_2 \rightarrow 1B_1$	51	0.035	$1B_1 \rightarrow 1B_2$	50	$1B_2 \rightarrow 1B_1$	50
24	0.057	462	b_{3u} (B_1)	0.023	0.024	$1A_1 \rightarrow 1B_1$	57	$1B_1 \rightarrow 1A_1$	42	0.029	$1A_1 \rightarrow 1B_1$	50	$1B_1 \rightarrow 1A_1$	50
23	0.072	583	b_{1u} (A_1)	0.002	0.002	$1B_1 \rightarrow 2B_1$	43	$2B_1 \rightarrow 1B_1$	57	0.002	$1B_1 \rightarrow 2B_1$	50	$2B_1 \rightarrow 1B_1$	50
21	0.088	713	b_{2g} (B_1)	0.014	0.008	$1A_1 \rightarrow 1B_1$	54	$1B_1 \rightarrow 1A_1$	46	0.01	$1A_1 \rightarrow 1B_1$	50	$1B_1 \rightarrow 1A_1$	50
20	0.098	790	a_g (A_1)	0.127	0.103	$1B_1 \rightarrow 1B_1$	97			0.121	$1B_1 \rightarrow 1B_1$	96		
19	0.102	826	b_{1g} (A_2)	0.01	0.008	$1B_1 \rightarrow 1B_2$	48	$1B_2 \rightarrow 1B_1$	52	0.009	$1B_1 \rightarrow 1B_2$	50	$1B_2 \rightarrow 1B_1$	50
18	0.104	836	b_{3u} (B_1)	0.008	0.004	$1A_1 \rightarrow 1B_1$	55	$1B_1 \rightarrow 1A_1$	45	0.005	$1A_1 \rightarrow 1B_1$	50	$1B_1 \rightarrow 1A_1$	50
17	0.125	1009	b_{2g} (B_1)	0.004	0.004	$1A_1 \rightarrow 1B_1$	62	$1B_1 \rightarrow 1A_1$	38	0.004	$1A_1 \rightarrow 1B_1$	50	$1B_1 \rightarrow 1A_1$	50
15	0.138	1114	a_g (A_1)	1.000	1.000	$1B_1 \rightarrow 1B_1$	100			1.000	$1B_1 \rightarrow 1B_1$	98.7		
13	0.161	1303	b_{1u} (A_1)	0.004	0.004	$1B_1 \rightarrow 2B_1$	49	$2B_1 \rightarrow 1B_1$	51	0.003	$1B_1 \rightarrow 2B_1$	50	$2B_1 \rightarrow 1B_1$	50
9	0.205	1656	a_g (A_1)	0.084	0.084	$1B_1 \rightarrow 1B_1$	100			0.073	$1B_1 \rightarrow 1B_1$	99.6		
8	0.212	1712	a_g (A_1)	0.531	0.509	$1B_1 \rightarrow 1B_1$	100			0.452	$1B_1 \rightarrow 1B_1$	99		

$$\text{Tr}[\Gamma_L G_0^r \alpha_q G_0^r \Gamma_R G_0^a \alpha_q G_0^a] = \text{Tr}\left[\Gamma_L \frac{\partial G_0^r}{\partial Q} \Gamma_R \frac{\partial G_0^a}{\partial Q}\right] \quad (15)$$

using $G_0^{r,a} \alpha_q G_0^{r,a} = \frac{\partial G_0^{r,a}}{\partial Q}$. This result is precisely that obtained by Troisi and Ratner[12,18] using a perturbation expansion of the elastic component of the current. Equation (15) puts this very useful expression in the context of a general theory for the nonequilibrium transport process and a hierarchy of numerical methods for obtaining the exact and approximate IETS intensities.

IV. FROM CHANNELS TO PROPENSITY RULES

Based on this simple formalism, the factors that lead to the propensity of different modes in IETS are depicted graphically in Fig. 4. The top part is a schematic plot of six characteristic normal modes and their frequencies. The second and third rows show the modulus of the eigenvectors of $(A^L)^*$ and A^R associated with the dominant channels through the coupling-weighted molecular density that indicate how transported charges enter and leave the molecular region. These left and right pairs of channels are coupled by a molecular vibronic coupling term $|\bar{\alpha}_{ij}^q|^2$ whose origin in terms of interfering atomic contributions and bond contributions is shown in the lower part of the figure. To do this, we expand

$$|\bar{\alpha}_{ij}^q| = \sum_E \sum_F \text{Re}(\beta_{EF} e^{-i\phi}), \quad (16)$$

where E and F refer to different atoms, ϕ is the phase of the complex number $\bar{\alpha}_{ij}^q$, and the atomic (diagonal) and bond (off-diagonal) contributions β are defined using

$$\beta_{EF} = \sum_{m \in E} \sum_{n \in F} (C_{im}^L)^* \alpha_{mn}^q C_{nj}^R, \quad (17)$$

where $C_{ij}^{L,R}$ are the elements of the eigenvectors and α_{mn}^q are the vibronic coupling matrix elements in the atomic-orbital basis. The off-diagonal elements of this coupling matrix represent scattering from the bonds of the molecule while the diagonal elements represent scattering off the atoms. Through chemical or other external modifications to the molecule, Fig. 4 indicates how the IETS propensities of different modes can be manipulated.

To show how the lower frames of Fig. 4 depict the molecular properties, the dominant contributions β_{EF} evaluated for the most intense IETS mode, ν_{15}, are given in Table III. The largest contribution (40 % of the total) arises from each of the two C-S bonds. The upper frames in Fig. 4 indicate why a large contribution arises from the C-S bonds: both the L- and R-channel eigenvectors contain components on these atoms, and the vibrational mode acts to change the C-S bond length. In the lower frame of Fig. 4, the thick and dark blue lines over the C-S bonds indicate this contribution graphically. From Table III, the next most important contribution is 19% and arises from each of the C-C$_o$ bonds, where C$_o$ is the carbon ortho to the linked carbon. In Fig. 4, the total intensity of blue color for the C-S and C-C$_o$ bonds indicates their relative importance. Blue coloring is used to indicate that the contributions from the C-S and C-C$_o$ bonds add constructively to enhance the inelastic current, their net effect being to generate $(2 \times 40)\% + (4 \times 19)\% = 158\%$ of the current. This exceeds 100% as the remaining minor contributions to the current, dominated as indicated in Table III by the atomic
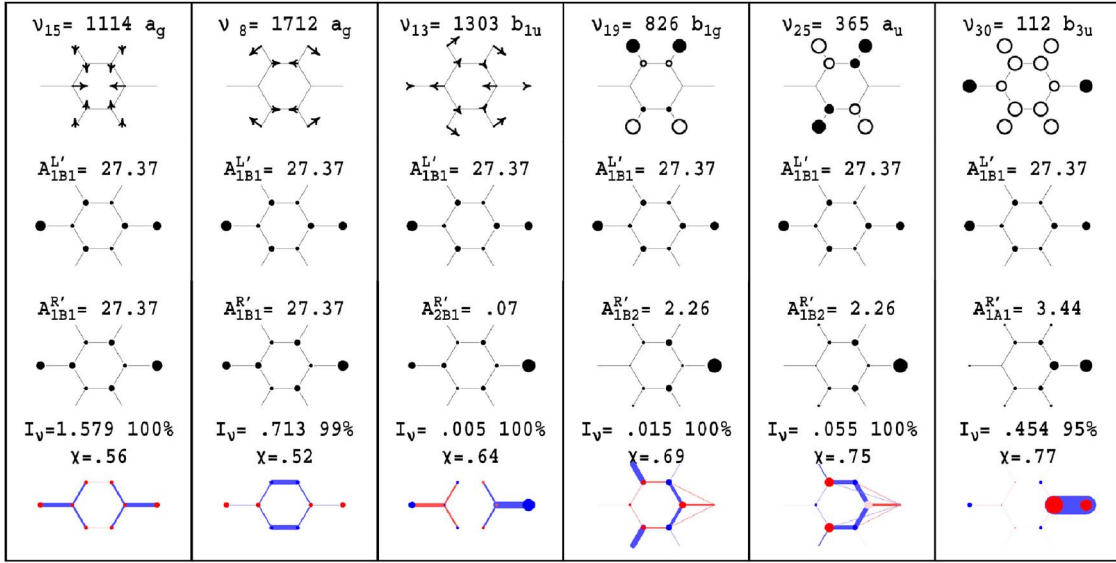
FIG. 4. (Color online) Diagrammatic description of the origin of the IETS intensity for six characteristic vibrational modes. First row: depictions of the normal modes, including either arrows for in-plane modes or open and solid circles for out-of-plane modes, along with the mode frequency in cm^{-1} and molecular symmetry. Second and third rows: circles indicating the absolute values of the atomic contributions to the dominant eigenvectors C_i^L of A^L and C_j^R of A^R along with the associated eigenvalues $\bar{A}_{ii}^L$ and $\bar{A}_{jj}^R$, in a.u., from Table I. Fourth row: origin of the vibronic term $\bar{\alpha}_{ij}^q$ that couples these channels expressed in terms of atomic contributions (circles) and bond contributions (lines) colored blue (dark gray) and red (light gray) to indicate constructively and destructively interfering processes, respectively; also indicated is the total inelastic conductance at E_F of the mode and the percentage contribution arising from the indicated coupled channels (doubled for non-totally-symmetric modes to account also for its symmetry-related counterpart) and the destructive interference indicator χ.

S (-8% each) and C (-4% each) contributions, act destructively to reduce the current. Contributions that act destructively are indicated in red in Fig. 4. The total color density shown in circles for the atomic contributions is scaled to that of the bond vectors.

For each mode depicted in Fig. 4, the impact of destructive interference between electron scattering pathways is quantified using the indicator

$$\chi = 1 - \frac{\left| \sum_{EF} \beta_{EF} \right|}{\sum_{EF} |\beta_{EF}|}, \tag{18}$$

which takes on the value of $\chi=0$ to indicate only constructive interference to $\chi \approx 1$, indicating strong destructive interference. Modes dominated by destructive interference are likely to be highly sensitive to external modifications through modulation of the interference. For the example of ν_{15} considered previously, bond scattering is opposed by atomic scattering so that χ is quite large at 0.56. Of all of the vibrational modes, this mode, the most intense mode, has one of the *lowest* values of χ, however, indicating that interference effects will in general limit the development of simple chemical models for IETS intensity.

From the analysis of the channels we can also define propensity rules. The most active modes are the a_g modes. Based on the notion that the most intense modes will be those that access the dominant $1B_1$ paths through each of the junction-weighted densities of states, the most active modes are expected to be of A_1 symmetry in the C_{2v} conductance point group. Such modes will have either a_g or b_{1u} symmetry in the full molecular point group d_{2h}. Indeed, a_g modes are found to be the most active ones, but b_{1u} modes are found to be very weak. To understand this differentiation, we note that the transmission eigenvectors $C_{1B1}^{L,R}$ associated with the left and right $1B_1$ channels can be represented as a sum of terms each with either a_g or b_{1u} symmetry:

$$C^{L,R} = \frac{1}{\sqrt{2}}(\psi_{a_g} \pm \psi_{b_{1u}}), \tag{19}$$

where the upper (lower) sign is for the left (right) eigenvector. Substituting Eq. (19) into Eq. (13) splits the sum into four terms:

TABLE III. Normalized atomic $(\beta_{EE}/\Sigma_{EF}|\beta_{EF}|)$ and bond $[(\beta_{EF}+\beta_{FE})/\Sigma_{EF}|\beta_{EF}|]$ contributions to the molecular vibrational couplings between input and output electron scattering channels, $|\bar{\alpha}_{ij}^q|$ from Eq. (16), as visualized in Fig. 4; contributions are shown for the sulfur (S), connected carbon (C), its ortho-carbon (C$_o$), and its symmetry-related neighbor (C$_{o'}$).

	S	C	C$_o$	C$_{o'}$
S	-0.08			
C	0.40	-0.03		
C$_o$	-0.01	0.19	-004	
C$_{o'}$	-0.01	0.02	-0.02	-0.04

$$\bar{\alpha}_{ij}^q = \frac{1}{2}(\psi_{a_g})^\dagger \alpha^q \psi_{a_g} - \frac{1}{2}(\psi_{b_{1u}})^\dagger \alpha^q \psi_{b_{1u}} + \frac{1}{2}(\psi_{a_g})^\dagger \alpha^q \psi_{b_{1u}}$$

$$- \frac{1}{2}(\psi_{b_{1u}})^\dagger \alpha^q \psi_{a_g}. \qquad (20)$$

The product of the three elements in Eq. (20) must be totally symmetric, so only the first two terms may be nonzero for a_g modes while only the last two terms are permissible for b_{1u} modes. For a_g modes, the two allowed terms differ fundamentally in nature from each other, facilitating an allowed net contribution. However, for the b_{1u} modes, the two nonzero contributions exactly cancel each other, preventing inelastic scattering involving the same input and output channels. Hence, the inelastic scattering for the b_{1u} mode ν_{13} shown in Fig. 4 involves two *different* B_1 channels $1B_1$ and $2B_1$, so that the b_{1u} modes thus behave in the same fashion as do all other non-totally-symmetric vibrations. Conceptual approaches that exploit the sparseness properties of Γ_L and Γ_R alone do lead to the primary propensity rule favoring totally symmetric IETS excitations.

The propensity rules derived by transforming the Γs parallel these propensity rules and can be thought of as arising through similar arguments and serve to identify the most active modes in IETS. However, through our complete description of the junction-weighted densities of states, we can also derive propensity rules for the next most active vibrations: these will be the ones associated with both the largest and the second largest eigenvalues $\bar{A}_{ii}^L$, in this case the $1B_1$ and $1A_1$ channels, respectively, which are coupled by modes of b_{3u} and b_{2g} symmetry. Indeed, modes of both of these symmetries are identified as being quite prolific in Fig. 2 and Table II. Of note is the fact that these modes are out-of-plane modes that do not have a components in the direction of the charge flow; rather, they scatter electrons and holes between σ and π channels.

Within each particular symmetry class, the most active modes are seen from Fig. 4 to be those that involve atomic motion on atoms that have large amplitudes in the coupling-weighted left and right channels. As a result, a wide variety of scattering paths through the molecule can be invoked. As described earlier, the most intense a_g mode ν_{15} from Fig. 4 is an in-plane ring deformation mode that embodies some C-S stretching character, and all parts of the molecule contribute to the scattering. Also shown in Fig. 4 is the nature and scattering origin for the next most prolific mode, the a_g CH bending mode ν_8. This mode is coupled to some C_o-$C_{o'}$ stretching character, and it is this that facilitates the inelastic scattering from the input $1B_1$ channel to the output $1B_1$ channel.

For the intense non-totally-symmetric modes that scatter charges between σ and π channels, the most active modes are found to be those with significant C and S involvement. The scattering is not generated symmetrically from each end of the molecule, as scattering between input and output channels of the same type is constrained to be, but instead is typically dominated by a single C-S bond. Typifying this behavior is ν_{30}, the b_{3u} mode that couples the two most conductive junction channels $1A_1$ and $1B_1$ (see Table I). Figure 4 shows that the input and output channels both have ampli-

tude on the one C-S bond while the out-of-plane vibration also has C-S amplitude, allowing the σ-π mixing to occur. This mode is indeed the third most active mode calculated for IETS (see Table II), but as the bottom frame of Fig. 4 indicates, the dominant scattering from the C-S bond is strongly opposed by scattering from the individual C and S atoms. Were it not for this interference, this vibrations would be even more prolific in the calculated IETS. The largest destructive interference found was for the related b_{3u} mode ν_{24} for which $\chi = 0.91$.

Finally, we consider the C-H out-of-plane modes ν_{19} (b_{1g}) and ν_{25} (a_u) that have the same form except for opposite end-to-end symmetry. These modes coupe the most prolific and third-most prolific molecule-weighted junction channels $1B_1$ and $1B_2$, but as can be seen from the forms of the channels shown in Fig. 4, very few atoms are active in both channels. Hence, the scattering is intrinsically weak and contains contributions from nonintuitive nonbonded 1,3- and 1,4-intermolecular interactions. While these modes are predominantly C-H in character, they do provide scattering through their weak C-C contamination.

V. CONCLUSIONS

In conclusion, two approaches have been investigated to analyze the IETS signal in a 1,4-benzenedithiol molecule chemisorbed between two gold leads in the context of a full general formalism for nonequilibrium elastic and inelastic conduction processes. In both approaches, the inelastic current is split into a small number of noninterfering contributions or channels. The first approach, based on the insight provided by Troisi and Ratner[12,18] that only a few paths through the junctions are accessible, involves transformation of the molecule-electrode couplings $\Gamma_{L,R}$ and reduces dramatically the complexity of the problem. However, detailed insight into the influence of the molecule on these paths is required before the method can be put to practical use in the determination of propensity rules. The second approach provides this insight automatically through the transformation of the $(A^L)^*$ and A^R matrices that depicts the density of states of the molecule coupled to the contacts.

Our transformation allows the dominant channels for electron or hole conduction through the junctions, channels of different symmetries, to be identified, leading to propensity rules based on the affect of the normal modes of vibration in scattering charges between these channels. As for molecules such as 1,4-benzenedithiol with dominant π-conduction character, the molecule-weighted junction channel $1B_1$ is very much more prolific than in any other channel. This leads to the first propensity rule that the totally symmetric modes (a_g) dominate IETS as only these can couple $1B_1$ from the left lead to $1B_1$ in the right lead. A similar propensity rule is expected for all molecules chemisorbed to gold through sulfur links, independent of the actual identity of the dominant channel. Weaker contributions to IETS are then identified from the nature of the next-most significant molecule-weighted junction channel eigenvalue(s), which for 1,4-benzenedithiol are found to be $1A_1$ and $1B_2$, leading to a propensity for b_{2g} and b_{3u} modes and b_{1g}

and a_u modes, respectively, in its IETS. Once these dominant channels are identified for modes of a particular symmetry type, the most active modes can be determined by examination of how the normal mode affects the atoms accessed by the appropriate molecule-weighted junction channels and the nature of the junction channels: the same atoms must be involved in each channel, and the vibration must perturb these atoms. For coupling between the $1B_1$ and $1B_2$ channels, few atoms are involved in both channels and so the IETS is weak, but the overlap between the $1B_1$ and $1A_1$ channels is large and hence the IETS is strong. These intense IETS modes involve the mixing of molecular σ and π character through out-of-plane C-S distortions. However, a more subtle feature acts to determine the final IETS intensities: the scattering amplitude can be decomposed in terms of interfering contributions associated with scattering from each atomic center and from each bond in the molecule, and this interference is in general large. A practical consequence of this is that chemical and other variations are likely to modulate the IETS intensity associated with particular modes of vibration. Our analysis thus provides simple and effective *a priori* means by which a very complex process involving no formal selection rules can be controlled and manipulated to achieve desired outcomes.

[1] A. Aviram and M. A. Ratner, Chem. Phys. Lett. **29**, 277 (1974).

[2] Ya M. Blanter and M. Bttiker, Phys. Rep. **336**, 1 (2000).

[3] A. Mitra, I. Aleiner, and A. J. Millis, Phys. Rev. B **69**, 245302 (2004).

[4] A. Pecchia, A. Di Carlo, A. Gagliardi, S. Sanna, T. Frauenheim, and R. Gutierrez, Nano Lett. **4**, 2109 (2004).

[5] W. Wang, T. Lee, I. Kretzschmar, and M. A. Reed, Nano Lett. **4**, 643 (2004).

[6] J. G. Kushmerick, J. Lazorcik, C. H. Patterson, R. Shashidhar, D. Seferos, and G. C. Bazan, Nano Lett. **4**, 639 (2004).

[7] R. C. Jaklevic and J. Lambe, Phys. Rev. Lett. **17**, 1139 (1966).

[8] K. W. Hipps and U. Mazur, J. Phys. Chem. **97**, 7803 (1993).

[9] N. Lorente, M. Persson, L. J. Lauhon, and W. Ho, Phys. Rev. Lett. **86**, 2593 (2001).

[10] N. Mingo and K. Makoshi, Phys. Rev. Lett. **84**, 3694 (2000).

[11] J. Kirtley, D. J. Scalopino, and P. K. Hansma, Phys. Rev. B **14**, 3177 (1976).

[12] A. Troisi and M. A. Ratner, Nano Lett. **6**, 1784 (2006).

[13] K. Makoshi and N. Mingo, Surf. Sci. **34**, 502 (2002).

[14] S. G. Tikhodeev and H. Ueba, Phys. Rev. B **70**, 125414 (2004).

[15] M. Galperin, A. Nitzan, M. A. Ratner, and D. R. Stewart, J. Phys. Chem. B **109**, 8519 (2005).

[16] M. Paulsson, T. Frederiksen, and M. Brandbyge, Nano Lett. **6**, 258 (2006).

[17] G. C. Solomon, A. Gagliardi, A. Pecchia, Th. Frauenheim, A. Di Carlo, J. R. Reimers, and N. S. Hush, J. Chem. Phys. **124**, 094704 (2006).

[18] A. Troisi and M. A. Ratner, J. Chem. Phys. **125**, 214709 (2006).

[19] A. Pecchia and A. Di Carlo, Rep. Prog. Phys. **67**, 1497 (2004).

[20] Th. Frauenheim, G. Seifert, M. Elstner, Th. Niehaus, C. Koeler, M. Amkreutz, M. Sternberg, Z. Hajnal, A. Di Carlo, and S. Suhai, J. Phys.: Condens. Matter **14**, 3015 (2002).

[21] Y. Meir and N. S. Wingreen, Phys. Rev. Lett. **68**, 2512 (1992).

[22] G. C. Solomon, A. Gagliardi, A. Pecchia, Th. Fraueheim, A. Di Carlo, J. R. Reimers, and N. S. Hush, J. Chem. Phys. **125**, 184702 (2006).

[23] A. Bilic, J. R. Reimers, and N. S. Hush, J. Chem. Phys. **122**, 094708 (2005).

[24] H. Kondoh, M. Iwasaki, T. Shimada, K. Amemiya, T. Yokoyama, T. Ohta, M. Shimomura, and S. Kono, Phys. Rev. Lett. **90**, 066102 (2003).

[25] M. G. Roper, M. P. Skegg, C. J. Fisher, J. J. Lee, V. R. Dhanak, D. P. Woodruff, and R. G. Jones, Chem. Phys. Lett. **389**, 87 (2004).

[26] G. C. Solomon, A. Gagliardi, A. Pecchia, Th. Frauenhiem, A. Di Carlo, J. R. Reimers, and N. S. Hush, Nano Lett. **6**, 2431 (2006).

[27] S. Datta, *Electronic Transports in Mesoscopic Systems* (Cambridge University Press, Cambridge, England, 1995).